Journal of Power Sources 255 (2014) 302–307

Contents lists available at ScienceDirect

Journal of Power Sources

journal homepage: www.elsevier.com/locate/jpowsour

Short communication

Evaluation of proton conducting BCY10-based anode supported cells by co-pressing method: Up-scaling, performances and durability

J. Dailly [a,*], M. Marrony [a], G. Taillades [b], M. Taillades-Jacquin [b], A. Grimaud [c], F. Mauvy [c], E. Louradour [d], J. Salmi [e]

[a] EDF-EIFER, Emmy-Noether-Strasse 11, 76131 Karlsruhe, Germany
[b] CNRS, Université de Montpellier, AIME, 87, Av. du Dr Schweitzer, 33608 Montpellier, France
[c] CNRS, Université de Bordeaux, ICMCB, 87, Av. du Dr Schweitzer, 33608 Pessac, France
[d] Céramiques Techniques Industrielles CTI, 382 Avenue du Moulinas, 30340 Salindres, France
[e] Marion Technologies, Parc Technologique Delta Sud, 09340 Verniolle, France

HIGHLIGHTS

- Commercial powders produced at kilogram scale have been analysed and used.
- The maximum power density of around 180 mW cm^{-2} is obtained at 600 °C on both sizes.
- The co-pressing method is only efficient at the laboratory scale.

ARTICLE INFO

Article history:
Received 23 September 2013
Received in revised form
29 November 2013
Accepted 17 December 2013
Available online 26 December 2013

Keywords:
Praseodymium nickelate
Yttrium-doped barium cerate
Co-pressing
Screen-printing
Up-scaling
Proton ceramic fuel cell

ABSTRACT

One of the main target of the French ANR CONDOR (2009–2011) project coordinated by EDF-EIFER was the elaboration of proton conducting $BaCe_{0,9}Y_{0,1}O_{3-\delta}$-based cells using processes suitable at industrial level. Thus, commercial powders produced at kilogram scale (anode, electrolyte and cathode) have been analysed and used. Then, elaboration of protonic ceramic half-cells by co-pressing method from 25 mm to 80 mm in diameter has been assessed in order to establish the suitability of this shaping method regarding industrial requirements. According to results, the co-pressing method is relevant for the elaboration of cells up to 40 mm in diameter (laboratory experiment). A sintering step was carried out to densify the electrolyte layer to get a gas-tight membrane. Nickelate-based cathodes were screen-printed and electrochemical performances of the final assembly have been measured. Electrical power up to 180 mW cm^{-2} at 600 °C has been obtained on both 25 and 40 mm cells.

1. Introduction

The high energy conversion efficiency and the low impact to the environment are part of great advantages of Solid Oxide Fuel Cells (SOFCs), which are promising devices for electricity generation. They convert directly the chemical energy from the fuel to electricity. However, most of technical issues of SOFCs remain the high operating temperatures (>700 °C), leading to accelerated ageing of materials. During the last ten years, Protonic Ceramic Fuel Cell has considerably attracted attention thanks to the lower temperature range (400–600 °C) and the interest of a better energy efficiency with the non-dilution of the fuel since the water is produced to the air electrode side.

Since Iwahara published in the 80's his work on protonic perovskites as electrolyte for fuel cells [1–4], many proton conducting oxide structures have been studied, like perovskites [5–11], based-perovskites (like $Ba_3Ca_{1,18}Nb_{1,82}O_9$ or $BaIn_{0,8}Ti_{0,2}O_{2,6}\square_{0,4}$) [12–15], ortho-niobates [16–18] and others candidates [19–22].

Now, most of protons conducting ceramic cell researches are devoted to the optimization of their performances and reliability. This aspect request notably the strict reduction of ohmic resistance of each interface layers by promoting very thin and dense electrolyte layer [23–26], a well-architecture anode functional layer to increase the triple-phase boundary (TPB) for hydrogen electrode reactions [27,28] and a good chemical compatibility and microstructure for air electrodes side [29–32].

* Corresponding author. Tel.: +49 721 61 05 13 52; fax: +49 721 6105 1332.
E-mail address: dailly@eifer.org (J. Dailly).

0378-7753/$ – see front matter © 2013 Elsevier B.V. All rights reserved.
http://dx.doi.org/10.1016/j.jpowsour.2013.12.082

But, until now, most of electrical performances related in the literature do refer to lab-scale size cell below 10 mm of diameter. Thus, no real investigations of efficient up scaling routes have been led until now in order to fit to the industrial requirements for the introduction of cells in stacks. This aspect appears fundamental to approach the stack manufacturing then the system integration key steps research in a reasonable term.

Here proposed is the assessment of co-pressing methods for an up-scaling of PCFC anode- supported cell manufacture. Microstructure and electrical performances of such cells are investigated.

2. Experimental

2.1. Powders

All samples were prepared using commercial powders (Marion Technologies®) produced at kilogram scale, listed below:

- Electrolytes: **$BaCe_{0,9}Y_{0,1}O_{3-\delta}$ (BCY10)**
- Anode (cermet): **NiO–$BaCe_{0,9}Y_{0,1}O_{3-\delta}$**
- Cathode: **$Pr_2NiO_{4+\delta}$**

2.2. Cells elaboration

The half cells were made by co-pressing of powders (at AIME laboratory and Céramiques Techniques Industrielles CTI®). In a first time, cermet spray-dried powder (NiO-BCY10) was pressed (100 MPa) into discs (~25–40–80 mm in diameter, 2 mm in thickness). Then, a given weight of electrolyte powder (BCY10) was sieved on the top of the anode discs in order to reach a homogeneous and reproducible thickness for all the samples, and then co-pressed at 150 MPa. The green half cells were sintered at 1350 °C for 10 h on a bed of anode powder in order to limit chemical pollution and geometrical deformation.

The cathode was made by screen-printing (at ICMCB and EIFER laboratories). The slurry was prepared using cathode-powder and 6 wt.% ethylcellulose in Terpineol. Two layers were screen-printed on half-cells, dried at 100 °C in a drying box and were then fired at 1150 °C for 2 h in air.

2.3. Characterization of the samples

Crystallographic phases were determined at room temperature by X-ray diffraction (INEL brand), in the $\theta/2\theta$ mode, using the Kα1Cu radiation. The phase identification was done using the software WPA.

The size distributions of powders dispersed in water are determined by dynamic laser light scattering using a Mastersizer 2000 apparatus (Malvern brand) using the Mastersizer 2000 5.12 F software.

In order to appreciate their TEC difference, dilatometric measurement were carried out on sintered material samples with a Netzsch DIL 402 PC from room temperature to 1000 °C with a heating rate of 5 °C min^{-1}.

The cell morphologies are evidenced by electron microscopy in the SEM mode in a field-emission scanning electron microscope.

2.4. Electrochemical test conditions

Single cells were tested in fuel cell testing systems at 600 °C with non-humidified hydrogen as fuel and compressed air as oxidant. Electrical contacts to the cell were made using platinum wires welded to the platinum meshes used as current collectors. AC impedance spectroscopy was obtained over the frequency range from 0.01 to 10^5 Hz under open-circuit conditions and under polarization.

3. Results and discussion

3.1. Characterization of powders

As shown in Figs. 1 and 2, the as-prepared powders of $BaCe_{0,9}Y_{0,1}O_{3-\delta}$ and $Pr_2NiO_{4+\delta}$ exhibit a well-developed crystallization and all the peaks can be well indexed as pure perovskite and Ruddlesden–Popper phases, respectively. It could be clearly seen that there is no evidence of the formation of other substances. All the XRD measurements made on the synthesized-phases are in agreement with the corresponding JCPDS card (n° 82–2372 for $BaCe_{0,9}Y_{0,1}O_{3-\delta}$, n° 44–1159 for NiO, n° 34–1113 for $Pr_2NiO_{4+\delta}$, respectively). The average crystallite sizes are listed in Table 1.

Dilatometric experiments were carried out on sintered samples in order to measure their thermal expansion coefficient (TEC), and evaluate the potential mechanical stresses during co-firing. Values are summarized in Table 2: even if the difference between TEC values are rather different, no layer delamination has been observed after cell elaboration, meaning that membrane and substrates are likely to compensate this gap.

3.2. Up-scaling of cells

In the first stage, NiO–$BaCe_{0,9}Y_{0,1}O_{3-\delta}$/$BaCe_{0,9}Y_{0,1}O_{3-\delta}$/$Pr_2NiO_{4+\delta}$ assemblies were prepared at lab-scale (i.e. 25 mm in diameter, Fig. 3). Microscopic observations of the cells before testing show a fully densified electrolyte (density higher than 95%, nearly 50 μm thick) which is well stuck on a homogeneous biphasic anode (Fig. 4). Figs. 5 and 6 also confirm that good planarity and crack-free assemblies can be obtained by simple manual deposition.

The up-scaling of cell fabrication consisted in improving the size of samples while using the same co-pressing method (Fig. 5). The microstructure remained the same (Figs. 4 and 6) and planar and crack-free assemblies have been also obtained.

The repartition of each element of 40 mm cells has been checked by Energy-dispersive X-ray spectroscopy mapping (Fig. 7). All elements are well dispersed and there is no evidence of nickel in the electrolyte. All the observation on 40 mm cells shows that the first up-scaling step was a success.

Up-scaling the size up to 80 mm in diameter brings more mechanical and technical problems, the most critical step being the deposition of the electrolyte: the bigger the cell is, the less the thickness of the electrolyte is homogeneous. Experience proved

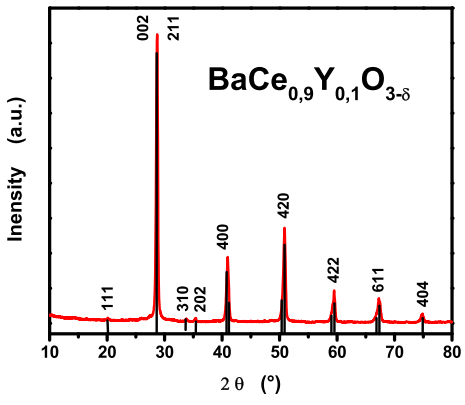

Fig. 1. XRD pattern for the $BaCe_{0,9}Y_{0,1}O_{3-\delta}$ powder.

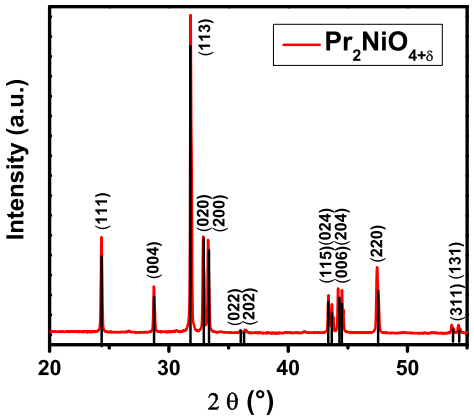

Fig. 2. XRD pattern for the $Pr_2NiO_{4+\delta}$ powder.

that it is very complicated to obtain manually a good repartition of the electrolyte powder on the surface of a large-scale anode substrate which leads obviously to a problem of reproducibility of cell elaboration (Fig. 8). Moreover, the non-homogeneous thickness of the electrolyte implies additional mechanical stress during the sintering step, resulting in cracks on the electrolyte layer (Fig. 9). No crack-free 80 mm cell has been successfully elaborated by using the manual co-pressing method. Wet chemical routes such as tape-casting could be more appropriated for the elaboration of large protonic-based anode supported cells [33].

3.3. Performances

All cells exhibit a good stability under open circuit condition at 600 °C (Fig. 10). Stable and high OCV (around 1.1 V near to the theoretical value) values show that $BaCe_{0,9}Y_{0,1}O_{3-\delta}$ based-electrolyte is well densified and have a good chemical stability under test conditions [34].

Fig. 11 presents the *I–V* and *I–P* curves of both 25 and 40 mm cells. *I–V* curves are nearly linear and it can deduce that the voltage drop of the cell is mainly coming from ohmic resistance fall across the electrolyte. The maximum power density of around 180 mW cm^{-2} is obtained at 600 °C for both sizes of cells which is a reasonable value regarding results from the literature measured on button-size cells, comprised between 100 and 400 mW cm^{-2} [35].

The total Area Specific Resistances of the cells (ASR_{cell}) were calculated from the slope of the *I–V* curves and are reported in Table 3. As expected, results are very similar for both sizes of cell.

Table 1
Average crystallite-size of each material.

Product	*d* (50) (μm)
$BaCe_{0,9}Y_{0,1}O_{3-\delta}$	1.50
NiO	0.58
$Pr_2NiO_{4+\delta}$	0.32

Table 2
Thermal Expansion Coefficient of up-scaled anode and electrolyte material.

Compound	TEC (10^{-6} K^{-1})
$Pr_2NiO_{4+\delta}$	13.60
$BaCe_{0,9}Y_{0,1}O_{3-\delta}$	9.97
NiO–$BaCe_{0,9}Y_{0,1}O_{3-\delta}$	13.03

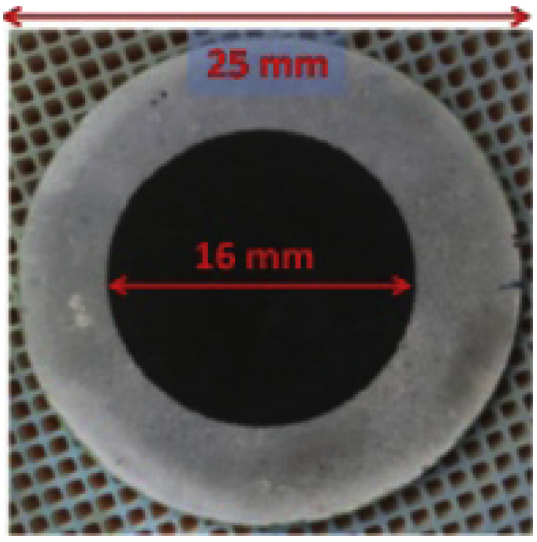

Fig. 3. Picture of a 25 mm cell.

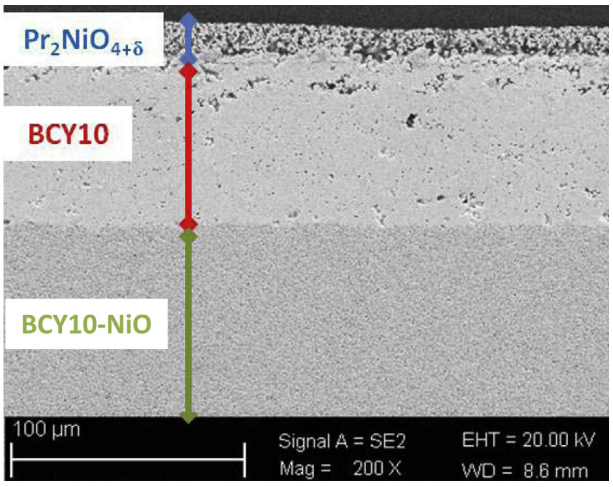

Fig. 4. Cross-sectional view of a 25 mm cell.

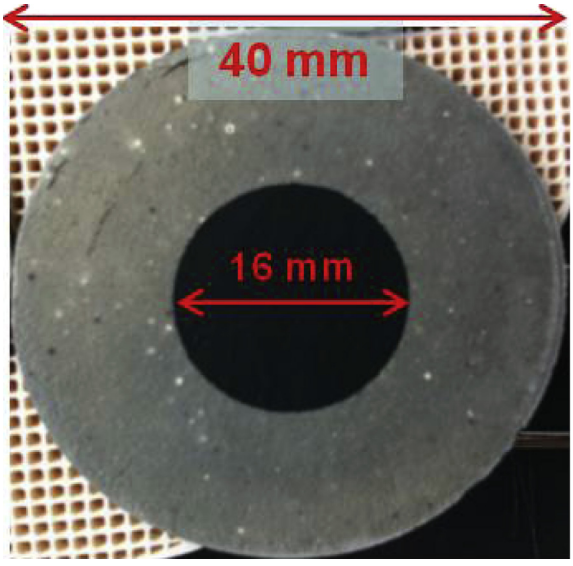

Fig. 5. Picture of a 40 mm cell.

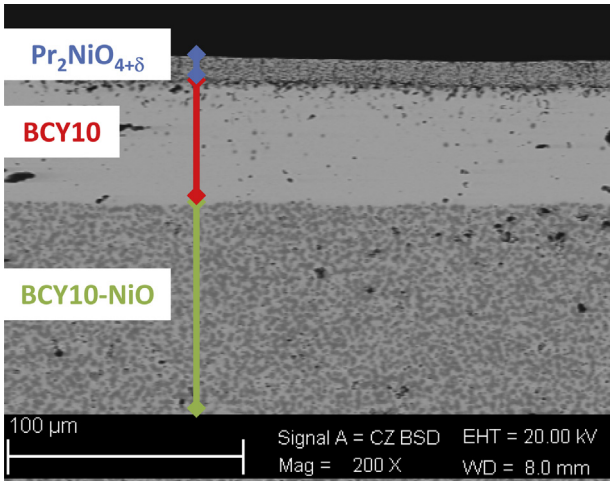

Fig. 6. Cross-sectional view of a 40 mm cell.

Impedance measurements were performed for both sizes of cell in order to study the electrochemical behaviour of the different layers. Fig. 12 shows typical Nyquist plots of the impedance data on a 40 mm Ni–$BaCe_{0,9}Y_{0,1}O_{3-\delta}$/$BaCe_{0,9}Y_{0,1}O_{3-\delta}$/$Pr_2NiO_{4+\delta}$ single cell at 600 °C. The high-frequency intercept corresponds to the ohmic resistance of the single cell (ASR_Ω), whereas the low-frequency intercept gives the total resistance of the cell ($ASR_{cell} = ASR_\Omega + ASR_P$). As shown in Table 3, ASR values obtained under dc conditions are in good agreement with electrochemical impedance spectroscopic measurements.

In order to study the stability of as-fabricated fuel cell, endurance tests were conducted and the evolution of the voltage has been recorded regarding time at 600 °C under constant current conditions 125 mA cm^{-2} (corresponding to an initial voltage of or 0.8 V) (Fig. 13). A continuous loss of the voltage is observed until 250 h, corresponding to an electrical degradation rate of 17% kh^{-1}. Then the potential of the cell fall to 0 V, corresponding probably to an irreversible modification of the microstructure of the cell. Other experiments have been performed with different current densities on both sizes of cells.

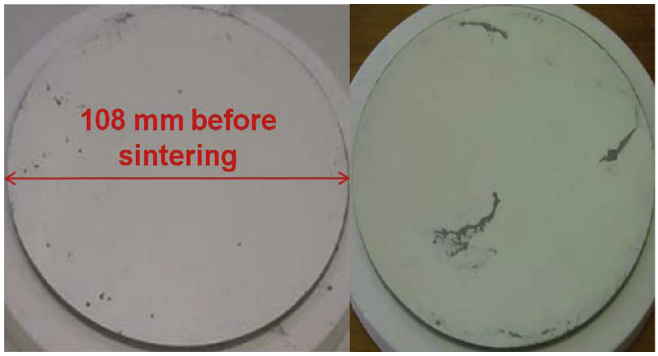

Fig. 8. Non-homogeneous repartition of electrolyte powder on up-scaled anode.

Whatever the current density and whatever the size of the sample, the cell reliability seems to be limited to few hundreds of hours. Indeed, a delamination of the cathode layer was mostly observed after all experiments, indicating a bad $Pr_2NiO_{4+\delta}$–$BaCe_{0,9}Y_{0,1}O_{3-\delta}$ interface and explaining the loss of the voltage.

Figs. 14 and 15 reveal typical image from Scanning Electron Microscope (SEM) of cross-sectional 25 and 40 mm cells after testing. The delamination of the cathode layer was highlighted, as well as the formation of an interfacial layer. Moreover, the porosity of the electrolyte seems to be higher than those obtained before testing, especially near to the cathode interface. Both effects could have been emphasized by the production of water vapour at the interface.

Once again, this aspect could be attributed to the reactivity phenomena observed between the two compounds, resulting in lowering the amount of Ce from the electrolyte in order to create the interlayer as already mentioned in our previous work [35–38]. This Ce-rich compound has been identified as the $Ce_{0,77}Pr_{0,23}O_{2-\delta}$ phase. The architecturization of the cathode layer using this compound as interlayer can neutralize the reactivity phenomena and increase the long-term stability of the cells. This topic is still under study.

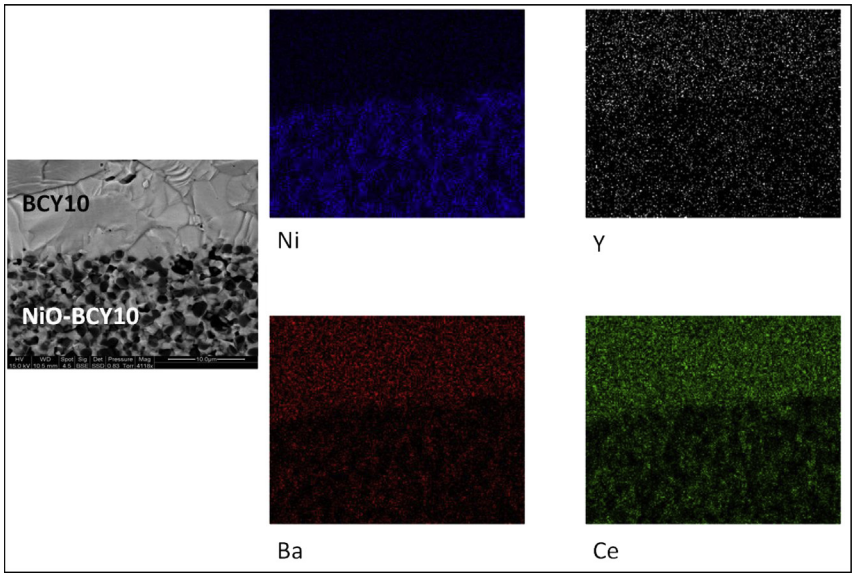

Fig. 7. Energy-dispersive X-Ray spectroscopy mapping of a 40 mm cell.

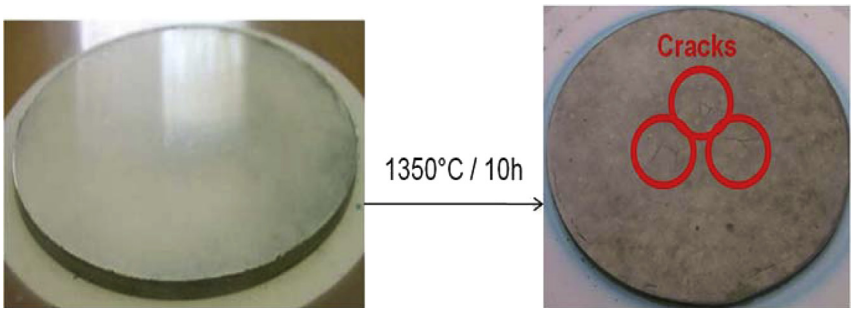

Fig. 9. Large-scale half-cell before and after sintering.

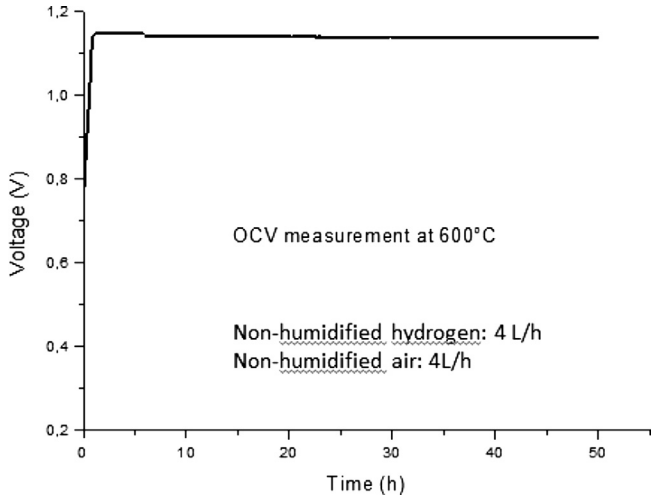

Fig. 10. Example of a long-term Open Circuit Voltage measurement of a 40 mm cell.

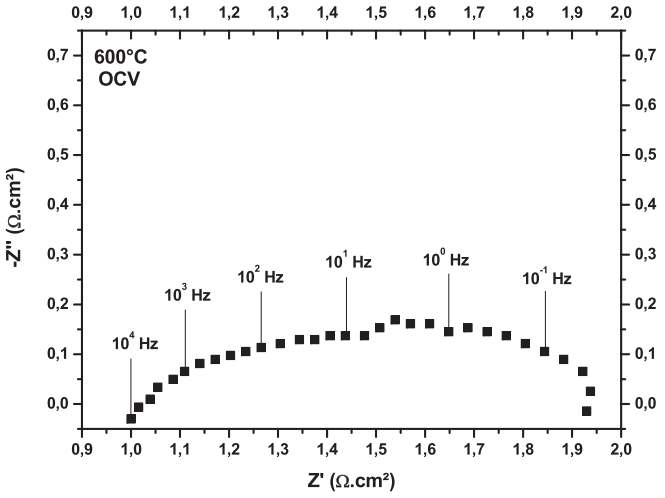

Fig. 12. Nyquist plots of a 40 mm Ni-BCY10/BCY10/$Pr_2NiO_{4+\delta}$ single cell at 600 °C.

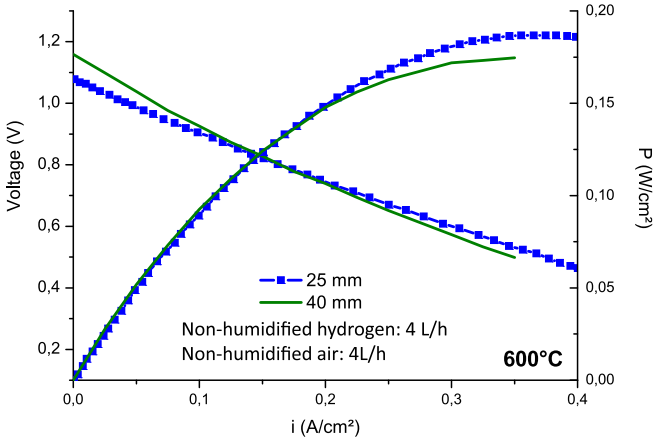

Fig. 11. *I–V* and *I–P* characteristics of 25 and 40 mm cells.

Table 3
I–V characteristics and power densities of the 25 and 40 mm cells on operation at 600 °C.

Size (mm)	Temp (°C)	OCV (V)	ASRcell @ OCV (Ω cm²)		ASR_Ω (Ω cm²)	ASR_P (Ω cm²)	P_{max} (mW cm⁻²)
			I–V slope	Impedance			
25	600	1.09	1.59	1.61	0.81	0.80	184
40	600	1.16	1.86	1.91	1.00	0.91	176

4. Conclusion

In this work, proton conducting ceramic oxide materials were synthesized. The up-scaling of powder synthesis at industrial scale was successfully performed, as well as increasing the size of cell from 25 to 40 mm in diameter. Afterwards, co-pressing method has been assessed to elaborate Proton conducting Ceramic Cells (PCC). Regarding feasibility and reproducibility, this shaping method is only efficient at the laboratory scale in order to evaluate

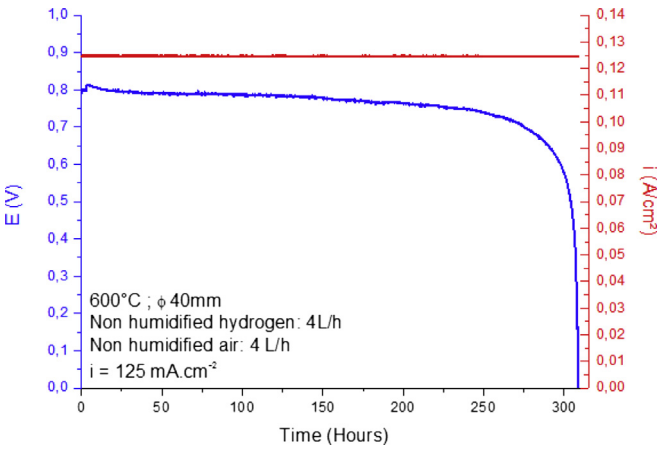

Fig. 13. Time dependent cell potential under constant polarization current density at 600 °C.

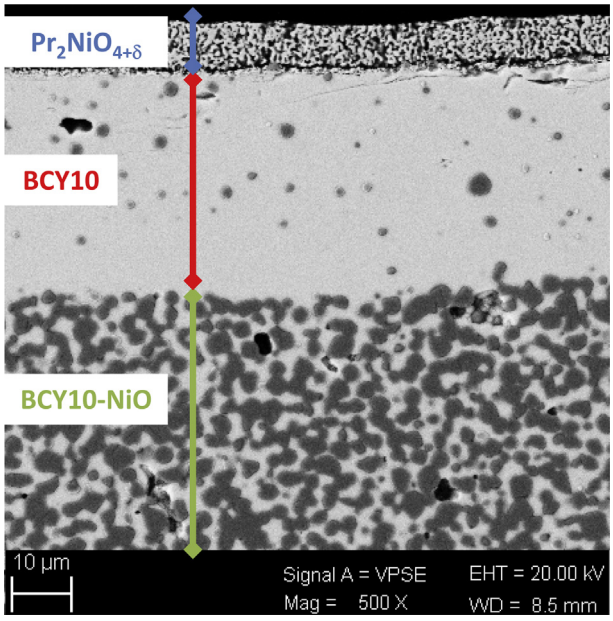

Fig. 14. SEM image of a cross-sectional view of a tested 25 mm cell.

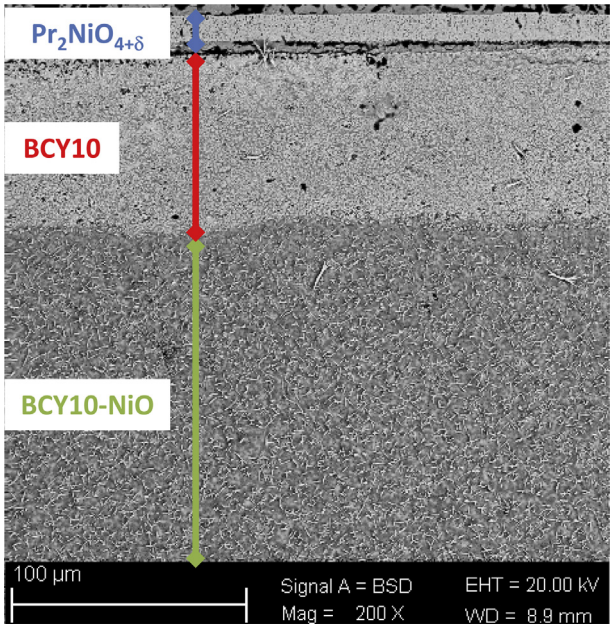

Fig. 15. SEM image of a cross-sectional view of a tested 40 mm cell.

quick performances of materials or assemblies and cannot guarantee an easy and reproducible manufacturing technique of PCC bigger than 40 mm of diameter, which is not compatible for an industrial way. Wet Chemical Routes are under investigation in order to reach larger cells size.

The cells show a maximal power density of 180 mW cm^{-2} at 600 °C for both sizes (25 and 40 mm). But a delamination of the cathode layer is observed which has limited the durability of cells in any case. A slight modification of the composition of the cathode compound or the addition of an interlayer should enhance the durability of nickelate/BCY10 – based PCC.

Acknowledgements

Funding by the Agence Nationale de la Recherche under the CONDOR project (ANR-08-PANH-004-01) is acknowledged with thanks. The authors would also like to thank industrial support from Flexitallic® and Fiaxell®.

References

[1] H. Iwahara, T. Esaka, H. Uchida, N. Maeda, Solid State Ionics 3–4 (1981) 359–363.
[2] H. Uchida, N. Maeda, H. Iwahara, Solid State Ionics 11 (1983) 117–124.
[3] H. Uchida, S. Tanaka, H. Iwahara, J. Appl. Electrochem. 15 (1985) 93–97.
[4] H. Uchida, H. Yoshikawa, H. Iwahara, Solid State Ionics 34 (1989) 103–110.
[5] K. Kreuer, W. Munch, M. Ise, T. He, A. Fuchs, U. Traub, J. Maier, Ber. Bunsenges. Phys. Chem. 101 (1997) 1344–1350.
[6] K. Katahira, Y. Kohchi, T. Shimura, H. Iwahara, Solid State Ionics 138 (2000) 91–98.
[7] M. Oishi, S. Akoshima, K. Yashiro, K. Sato, T. Kawada, J. Mizusaki, Solid State Ionics 181 (2010) 1336–1343.
[8] M. Oishi, S. Akoshima, K. Yashiro, K. Sato, J. Mizusaki, T. Kawada, Solid State Ionics 180 (2009) 127–131.
[9] P. Babilo, S. Haile, J. Am. Ceram. Soc. 88 (2005) 2362–2368.
[10] X. Xu, S. Tao, J. Irvine, J. Solid State Chem. 183 (2010) 93–98.
[11] E. Fabbri, A. D'Epifanio, E. Di Bartolomeo, S. Licoccia, E. Traversa, Solid State Ionics 179 (2008) 558–564.
[12] H.G. Bohn, T. Schober, T. Mono, W. Schilling, Solid State Ionics 117 (1999) 219–228.
[13] S. Valkenberg, H. Bohn, W. Schilling, Solid State Ionics 97 (1997) 511–515.
[14] J. Goodenough, J. Ruiz-Diaz, Y. Zhen, Solid State Ionics 44 (1990) 21–31.
[15] E. Quarez, S. Noirault, M.T. Caldes, O. Joubert, J. Power Sources 195 (2010) 1136–1141.
[16] R. Haugsrud, B. Ballesteros, M. Lira-Cantu, T. Norby, J. Electrochem. Soc. 153 (8) (2006) 87–90.
[17] R. Haugsrud, T. Norby, Solid State Ionics 177 (2006) 1129–1135.
[18] R. Haugsrud, T. Norby, J. Am. Ceram. Soc. 90 (2007) 1116–1121.
[19] K. Amezawa, S. Kjelstrup, T. Norby, Y. Ito, J. Electrochem. Soc. 145 (1998) 3313–3319.
[20] T. Norby, Solid State Ionics 125 (1999) 1–11.
[21] S. Noirault, S. Célérier, O. Joubert, M. Caldes, Y. Piffard, Inorg. Chem. 46 (2007) 9961–9967.
[22] S. Noirault, S. Célérier, O. Joubert, M. Caldes, Y. Piffard, Adv. Mater. 19 (2007) 867–870.
[23] A. Essoumhi, G. Taillades, M. Taillades-Jacquin, D.J. Jones, J. Rozière, Solid State Ionics 179 (2008) 2155–2159.
[24] Z. Khani, M. Taillades-Jacquin, G. Taillades, M. Marrony, D.J. Jones, J. Rozière, J. Solid State Chem. 182 (2009) 790–798.
[25] B. Lin, S. Wang, X. Liu, G. Meng, J. Alloys Compd. 478 (2009) 355–357.
[26] S. Wang, L. Zhang, L. Zhang, K. Brinkman, F. Chen, Electrochim. Acta 87 (2013) 194–200.
[27] Y.-E. Park, H.-I. Ji, B.-K. Kim, J.-H. lee, H.-W. Lee, J.-S. Park, Ceram. Int. 39 (2013) 2581–2587.
[28] B.H. Rainwater, M. Liu, M. Liu, Int. J. Hydrogen Energy 37 (2012) 18342–18348.
[29] J. Dailly, S. Fourcade, A. Largeteau, F. Mauvy, J.C. Grenier, M. Marrony, Electrochim. Acta 55 (2010) 5847–5853.
[30] C. Yang, Q. Xu, J. Power Sources 212 (2012) 186–191.
[31] E. Quarez, K.V. Kravchyk, O. Joubert, Solid States Ionics 216 (2012) 19–24.
[32] X. Lu, Y. Chen, Y. Ding, B. Lin, Int. J. Hydrogen Energy 37 (2012) 8630–8634.
[33] J. Dailly, M. Marrony, J. Power Sources 240 (2013) 323–327.
[34] M. Zunic, L. Chevalier, A. Radojkovic, G. Brankovic, Z. Brankovic, E. Di Bartolomeo, J. Alloys Compd. 509 (2011) 1157–1162.
[35] G. Taillades, J. Dailly, M. Taillades-Jacquin, F. Mauvy, A. Essouhmi, M. Marrony, C. Lalanne, S. Fourcade, D.J. Jones, J.-C. Grenier, J. Rozière, Fuel Cells 10 (2010) 166–173.
[36] J. Dailly, Ph.D. thesis, Université Bordeaux 1, 2008.
[37] A. Grimaud, Ph.D. thesis, Université Bordeaux 1, 2011.
[38] J. Dailly, F. Mauvy, M. Marrony, M. Pouchard, J.-C. Grenier, J. Solid State Electrochem. 15 (2011) 245–251.